J Neuropathol Exp Neurol
Vol. 74, No. 3
March 2015
pp. 273–285

ORIGINAL ARTICLE

OPEN

Cellular Mechanisms of Toll-Like Receptor-3 Activation in the Thalamus Are Associated With White Matter Injury in the Developing Brain

Regina Vontell, MSc, Veena Supramaniam, PhD, Josephine Wyatt-Ashmead, MD, Pierre Gressens, MD, PhD, Mary Rutherford, MD, Henrik Hagberg, MD, PhD, and Claire Thornton, PhD

Abstract

Toll-like receptor-3 (TLR3) has been identified in a variety of intracellular structures (e.g. endosomes and endoplasmic reticulum); it detects viral molecular patterns and damage-associated molecular patterns. We hypothesized that, after white matter injury (WMI) has occurred, localization and activation of TLR3 are altered in gray matter structures in response to damage-associated molecular patterns and activated glia. Therefore, we investigated the subcellular localization of TLR3 and its downstream signaling pathway in postmortem brain sections from preterm infants with and without WMI (7 patients each). We assessed astroglia (glial fibrillary acidic protein–positive), microglia (ionized calcium-binding adaptor molecule-1–positive), and neuronal populations in 3 regions of the thalamus and in the posterior limb of the internal capsule and analyzed TLR3 messenger RNA and protein expression in the ventral lateral posterior thalamic region, an area associated with impaired motor function. We also assessed TLR3 colocalization with late endosomes (lysosome-associated membrane protein-1) and phagosomal compartments in this region. Glial fibrillary acidic protein, ionized calcium-binding adaptor molecule-1, and TLR3 immunoreactivity and messenger RNA expression were increased in cases with WMI compared with controls. In ventral lateral posterior neurons, TLR3 was colocalized with the endoplasmic reticulum and the autophagosome, suggesting that autophagy may be a stress response associated with WMI. Thus, alterations in TLR3 expression in WMI may be an underlying molecular mechanism associated with impaired development in preterm infants.

Key Words: Interferon regulatory factor-3, Microtubule-associated protein light chain, Toll-like receptor-3, White matter injury.

INTRODUCTION

Preterm infants have high rates of white matter injury (WMI) with altered white matter development and associated reduced volume of gray matter structures (1–5). Numerous imaging and pathologic studies have demonstrated thalamic injury and subsequent atrophy within the developing white matter (5–9). Imaging studies on preterm infants with overt WMI have identified reduced thalamic volumes in medial dorsal (MD) and pulvinar regions, which have been correlated with long-term impairment in cognitive function in working memory and a decline in verbal intelligence (5, 8, 10).

Alongside hypoxia-ischemia, infection and inflammation are important contributors to the etiology of acquired injuries in the developing brain (11–13). The first line of defense for the detection and elimination of pathogens is provided by the innate immune system. Pathogen-associated molecular patterns or endogenous molecules (damage-associated molecular patterns [DAMPs]) released in response to injury are recognized by Toll-like receptors (TLRs), which are members of the pattern recognition receptor family (14). Thus, TLRs are capable of recognizing both exogenous pathogens and certain endogenously produced stimuli that are produced after injury (15, 16). TLR3 is a type I transmembrane receptor that recognizes exogenous double-stranded RNA (dsRNA). All TLRs are synthesized in the endoplasmic reticulum (ER) and are secreted on stimulation; most TLRs reside on the cell surface, but TLR3, TLR7, and TLR9 migrate to endosomes through the action of UNC93B1 (17–19). Once there, TLR3 recognizes its dsRNA ligand and activates a cascade of events mediated by the adaptor protein

From the Centre for the Developing Brain, Division of Imaging Sciences, and Biomedical Engineering, King's College London, King's Health Partners, St Thomas' Hospital (RV, VS, PG, MR, HH, CT); and Wigglesworth Perinatal Pathology Services, St Mary's Hospital (JW-A), London, United Kingdom; Perinatal Center, Departments of Physiology and Neuroscience and Clinical Sciences, Sahlgrenska Academy, Gothenburg University, Gothenburg, Sweden (HH); and Inserm, U676, Paris, France (PG).

Send correspondence and reprint requests to: Regina Vontell, MSc, Perinatal Imaging and Health, King's College London, First Floor, South Wing, St Thomas' Hospital, London SE1 7EH, United Kingdom; E-mail: regina.vontell@kcl.ac.uk

Mary Rutherford, Henrik Hagberg, and Claire Thornton share senior authorship.

This work was supported by the UK Medical Research Council strategic award (Grant No. P19381), the Wellcome Trust (Grant No. WT094823), Leducq Foundation, Swedish Medical Research Council (Grant No. VR 2012-3500), the Wilhelm and Martina Lundgren Foundation, the Åhlén Foundation, the Frimurare Barnhus Foundation, the Byggmästare Olle Engqvist Foundation, The Brain Foundation (Grant No. 2013-0035), and Governmental Grants for University Hospitals in Sweden (Grant No. ALFGBG-137601). The authors acknowledge financial support from the Department of Health via the National Institute for Health Research Comprehensive Biomedical Research Center award to Guy's and St Thomas' NHS Foundation Trust in partnership with King's College London and King's College Hospital NHS Foundation Trust.

Supplemental digital content is available for this article. Direct URL citations appear in the printed text and are provided in the HTML and PDF versions of this article on the journal's Web site (www.jneuropath.com).

Toll/IL-1–inducing interferon-β nuclear (20). Toll/IL-1–inducing interferon-β nuclear interacts with Tank binding kinase-1, resulting in the phosphorylation and nuclear translocation of interferon regulatory factor-3 (IRF-3) and the subsequent production of type I interferons. Toll/IL-1–inducing interferon-β nuclear also binds to tumor necrosis factor receptor–associated factor-6, ultimately activating transcription mediated by nuclear factor κ light chain enhancer of activated B cells (21).

Toll-like receptor-3 responses to endogenous DAMPs and the versatile roles they play in development are areas of intense investigation. Recent studies have suggested that RNA released from either damaged tissue or dying cells serves as ligands for TLR3, triggering necrotic or apoptotic pathways and the canonical TLR3 pathway (22–24). Furthermore, in the developing brain, TLR3 may negatively regulate neural progenitor cell proliferation and neurite development (25). Thus, TLR3 activation may influence neuron fate during fetal development (26). Indeed, it was recently shown that TLR3 sensitizes the brain to hypoxic-ischemic injury (27), and TLR3 activation with polyinosine:polycytidylic acid (synthetic dsRNA) during early fetal life produces behavioral problems resembling autism and schizophrenia in animal models (28, 29).

Identification of TLR3 in neurons and glial intracellular structures is important in fully comprehending neuronal dysfunction after WMI because TLR3 could respond to endogenous damage signals and may influence premature collapse of neurons with resultant atrophy of gray matter structures (22).

Previously, we showed that glia and neuronal TLR3 expression was upregulated in response to periventricular WMI in the frontal lobes of human preterm infants (30). We also found that cellular density in the cortex was significantly lower, with an increase in neuronal number, in the periventricular white matter in WMI cases indicating migration interference. Medial dorsal and ventral lateral thalamic axons extend into the white matter regions of the orbital medial and dorsal lateral frontal lobes, respectively. Thus, these nuclei are more susceptible to injury because these are the sites where periventricular infarcts occur, and they may impair motor and cognitive pathways. Here we extend our study to examine the localization and cellular mechanisms of TLR3 in areas of the thalamus. Our findings may have implications for the health of thalamocortical connections after WMI.

MATERIALS AND METHODS

A written informed parental consent form was acquired according to National Health Service UK guidelines. Study ethics approval was obtained from the National Research Ethics Service (West London) UK (ethics number 07/H0707/139; Postmortem Magnetic Imaging Study of the Developing Brain). Fourteen extremely preterm postmortem brains (<32 weeks' gestational age) of vaginally delivered neonates were used in this study. The primary cause of death of each case was assessed by a pathologist (Josephine Wyatt-Ashmead). Amniotic fluid infections were identified in most of the cases; however, none of the cases had leptomeningitis or vascular thrombosis. Seven of the brains showed no significant brain pathology on gross and microscopic examination from postmortem examination and had no visible brain abnormalities on postmortem magnetic resonance imaging. These were used as nonneuropathologic controls (control cases). The remaining 7 brains showed cerebral white matter gliosis, lipid-laden macrophages, and focal lesions with evidence of WMI on pathologic examination (WMI cases). Cases with known cortical maldevelopment and germinal matrix hemorrhages were excluded from this study. Case details, tissue preparation, and magnetic resonance imaging analyses have already been described (30) and are summarized in Data, Supplemental Digital Content 1, http://links.lww.com/NEN/A703.

Tissue Preparation

The bodies were refrigerated (2°C–4°C) before postmortem examination, and whole postmortem brains were fixed in 4% formalin for 5 to 7 weeks depending on size. The whole brains were sliced prospectively for this study by a pathologist (Josephine Wyatt-Ashmead) on the neural axis, which included key anatomic regions based on specific landmarks. The tissue blocks were processed on a Bright Tissue Processor (Bright Instrument Co Ltd, Cambridgeshire, United Kingdom). Paraffin-embedded tissue blocks were sectioned at 6 μm using a Leica RM2245 microtome (Leica Microsystems UK Ltd, Buckinghamshire, United Kingdom). Paraffin-embedded tissue sections from the cerebral hemispheres at the level of the globus pallidus were used for immunohistochemistry.

Immunohistochemistry and Immunofluorescence

Standard immunohistochemistry procedures for these brain sections have been described previously (30). Primary antibodies, dilutions and sources, and species-appropriate secondary antibodies are listed in Table 1.

Microscopy and Quantitative Analyses

Unbiased counts of TLR3-immunopositive, glial fibrillary acidic protein (GFAP)–immunopositive, and ionized calcium-binding adaptor molecule-1 (Iba-1)–immunopositive cells and the averaged cell density (hematoxylin positive nuclei/mm^2) were obtained using the CM1 and CM2 modules for virtual tissue scan (MicroBrightfield Inc, Colchester, VT) using stereology software (Stereo Investigator version 8.27; MicroBrightfield Inc). The average area of each contour was encompassed by a 2.1-mm^2 region, which was made using a 5× objective microscope, to provide an average of 40 high-power field images per scan collected using a 40× objective microscope (0.0426 mm^2); counts were automated using the program Image Pro Premier (Media Cybernetics, Warrendale, PA). In the pilot study, the counting profile described previously counted the correct number of labeled cells and nuclei (using an Image J cell counter).

Three thalamic regions were determined by the cellular architecture described (31, 32): the MD nuclei lateral to the internal medullary lamina, the ventral lateral posterior (VLp) nuclei medial to the external globus pallidus, and the ventral posterior lateral (VPL) nuclei medial to the internal globus pallidus. In addition, 2 regions—posterior limb of the internal capsule (PLIC) adjacent to the VLp (PLIC-VLp) and PLIC adjacent to the VPL (PLIC-VPL)—were investigated. Sampling areas

TABLE 1. Primary and Secondary Antibodies Used for Immunolabeling

Antigen	Catalog Number	Source	Species	Concentration	Target
TLR3	ab62566	Abcam (Cambridge, United Kingdom)	Rabbit	0.1 μg/mL	TLR3
GFAP clone G-A-5	G3893	Sigma-Aldrich Co Ltd	Mouse	1 μg/mL	Astrocytes and radial glial cells
Iba-1	019-19741	Wako Chemicals GmbH (Osaka, Japan)	Rabbit	5 ng/mL	Microglia and macrophages
Vesicular glutamate transporter-1	ab79774	Abcam	Sheep	1 μg/mL	Vesicular glutamate transporter-1
Glutamate decarboxylase-67	ab26116	Abcam	Mouse	1 μg/mL	GABAergic nuclear marker
Vesicular GABA transporter	131 011	Synaptic Systems GmbH (Gottingen, Germany)	Mouse	1 μg/mL	GABAergic processes
Early endosome antigen-1	E7659	Sigma-Aldrich Co Ltd	Mouse	1 μg/mL	Early endosomal marker
LAMP-1	ab3298	Abcam	Mouse	2.5 μg/mL	Late endosomal/lysosome marker
Calreticulin	LSB3131	LifeSpan Biosciences (Nottingham, United Kingdom)	Chicken	1 μg/mL	ER lumen
LC-3-II	ab65054	Abcam	Sheep	5 μg/mL	Autophagosomal vacuoles (autophagosome)
Mitochondrial antigen	ab3298	Abcam	Mouse	0.5 μg/mL	Mitochondrial antigen
IRF-3	sc-15991	Santa Cruz Biotechnology (Santa Cruz, CA)	Goat	10 μg/mL	IRF-3
NeuN	ABN90P	Millipore (Temecula, CA)	Guinea pig	0.3 μg/mL	Postmitotic neurons
HuC/HuD	A21271	Life Technologies	Mouse	2.5 μg/mL	All neurons (newly differentiated, mature)
Biotinylated antibody	BA2000	Vector Laboratories (Burlingame, CA)	Mouse	7.5 μg/mL	
Biotinylated antibody	BA1000	Vector Laboratories	Rabbit	7.5 μg/mL	
ABC kit	PK6200	Vector Laboratories	Universal	1:200	Secondary antibodies for immunofluorescence
Alexa Fluor 488	A10684	Life Technologies	Mouse	4 μg/mL	
Alexa Fluor 488	A21202	Life Technologies	Mouse	4 μg/mL	
Alexa Fluor 488	A11039	Life Technologies	Chicken	4 μg/mL	
Alexa Fluor 488	A11055	Life Technologies	Goat	4 μg/mL	
Alexa Fluor 488	A11015	Life Technologies	Sheep	4 μg/mL	
Alexa Fluor 546	A11010	Life Technologies	Rabbit	4 μg/mL	
Alexa Fluor 546	A10040	Life Technologies	Rabbit	4 μg/mL	
Alexa Fluor 647	A21450	Life Technologies	Guinea pig	4 μg/mL	
IRDye 800			Mouse	1 μg/mL	

and strategies for identifying regions of interest are shown using a standard hematoxylin-and-eosin stain (Fig. 1A).

All cells (identified by hematoxylin counterstain) were counted in MD, VLp, and VPL thalamic nuclei and in adjacent PLIC regions for every stain. After the nuclei had been counted, the cellular densities of GFAP-immunopositive and Iba-1–immunopositive cells were quantified by the first author (Regina Vontell) and a student volunteer (Megan Holly Atkins) who were blinded to case data. Tissue scans were reviewed (by Regina Vontell) to ensure that the glia had met the criteria (e.g. hematoxylin-positive nucleus [<10 μm^2] and GFAP-positive cytoplasm) to avoid duplicate counts. Neuronal counts were performed using track-and-trace morphometry data analysis. In brief, after the cells had been counted, we identified those cells that were HuC/HuD-immunopositive using tracking data analysis (Image Pro Premier; Media Cybernetics).

For glial and neuronal investigations, data were normalized by using the ratio of immunopositive cells to the entire population (hematoxylin-positive) . The area of TLR3 immunoreactivity was determined by dividing each TLR3 scan into 4 equal quadrants (500 μm^2) using the Image Pro Premier parent-child application (Image Pro Premier; Media Cybernetics). We defined the nucleus and the cytoplasm (''parent'') and averaged the measured area (μm^2) of TLR3 immunoreactivity (''child'') detected per cell for each of the thalamic and PLIC regions (33).

Data were analyzed using 1-way analysis of variance followed by the Tukey multiple comparison test to compare ratios in different thalamic nuclei and different regions of PLIC between groups (WMI compared with controls). Data are presented as mean ± SE; significance was set at $p < 0.05$. All statistical analyses were performed using GraphPad Prism 6.0 (GraphPad Software, San Diego, CA).

Cellular localization of TLR3 was performed via semiquantitative analysis through the center of the contour of the VLp region (Fig. 1A) because this thalamic region has neurons with the largest cell bodies and thick fibrous axons. An average of 8 confocal double-labeled and triple-labeled microphotographs per case were captured for each analysis using a Leica SP5 spectral confocal microscope. Microscope settings were appropriate for the fluorophores present, using a 63× objective (0.00598 mm^2) to provide an average resolution of 75 nm, which allowed for optimal oversampling of the structures of interest. Colocalization was tested with Image J version 1.42 (National Institutes of Health, Bethesda, MD) at 3 points

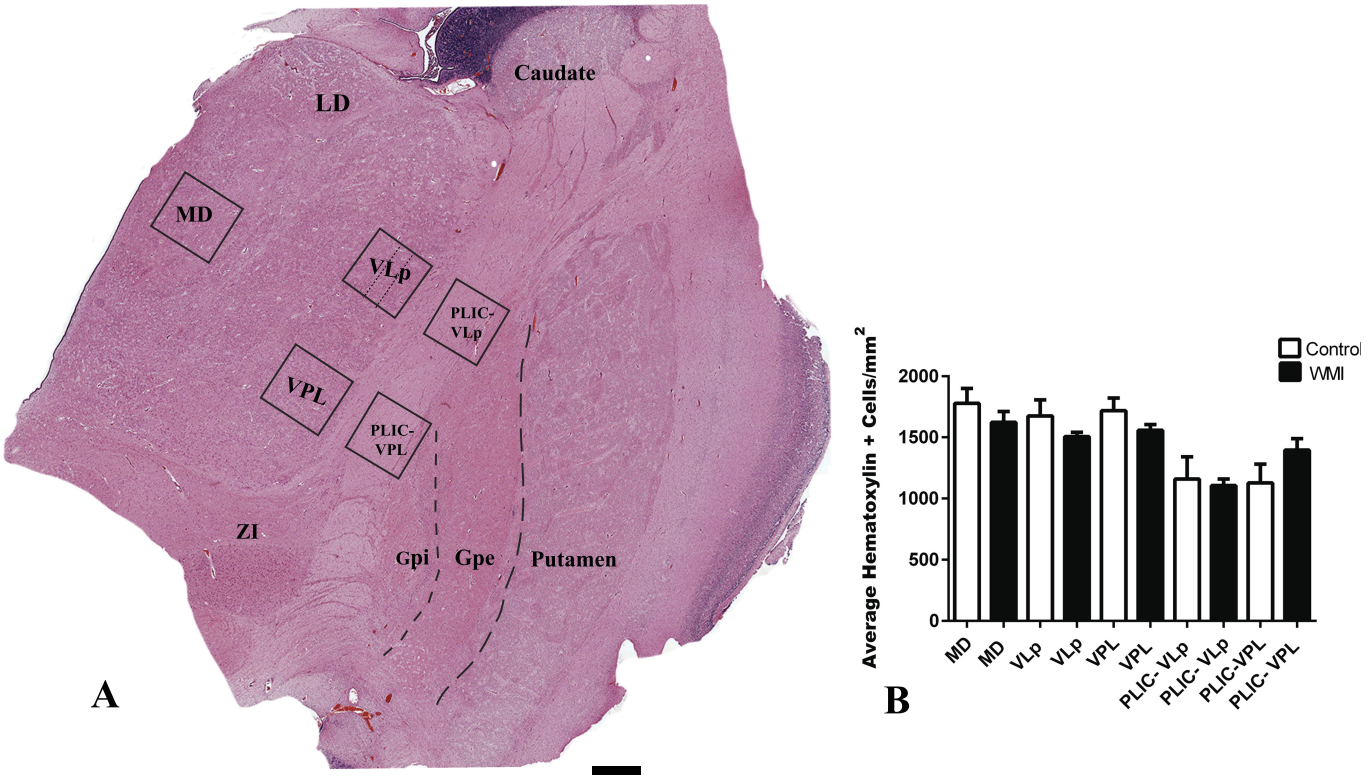

FIGURE 1. Global view of the thalamus. **(A)** The strategies for the quantification of different cell populations and TLR3 expression are demonstrated in Control 7 (28.2 weeks' gestational age). Boxes represent the contours made in MD, VLp, and VPL thalamic nuclei and in PLIC-VLp and PLIC-VPL. Throughout the study semiquantitative analyses were performed in the VLp region (dotted lines in VLp). **(B)**The (averaged) cell density (hematoxylin positive nuclei/mm^2) in MD, VLp, and VPL thalamic nuclei or in PLIC regions did not significantly differ between controls and WMI cases. Scale bar = 1,000 μm. GPe, globus pallidus externa; GPi, globus pallidus interna; LD, lateral dorsal; ZI, zona incerta.

in the z-stack of each image by a student volunteer (Chloe Suzanne Atkins) who was blinded to case data. All colocalization duals performed were first evaluated using the Costes approximation test, which determined whether all randomized images had worse correlation than real images to assure that the similarity of shapes between 2 images was not attributable to chance. We continued with the Mander's correlation analysis. Data were analyzed with Student *t*-test using a Mann-Whitney post hoc test between groups (WMI compared with controls) in the VLp thalamus. Data are presented as mean ± SD; significance was set at $p < 0.05$. All statistical analyses were performed using GraphPad Prism 6.0.

Translocation of IRF-3 signal from the cytoplasm to the nucleus was determined using the Image Pro Premier parent-child application (Image Pro Premier; Media Cybernetics). In brief, each case had an average of 50 nuclei (obtained using a 63× objective on the confocal microscope) in the VLp region of the thalamus (Fig. 1A). The nuclear boundary was determined by DAPI staining, and the threshold was maximized to achieve a solid object (''parent''). Next, IRF-3 intensity was averaged using Leica-LAS Lite report for each stack in all of the cases (i.e. WMI and controls). The average IRF-3 signal intensity was used to set the threshold minimum and maximum to register how much signal (''child'') was found in each nucleus (33).

In Situ Hybridization

Human TLR3 complementary DNA was cloned from human brain total RNA by reverse transcription–polymerase chain reaction (Multiscribe; Applied Biosystems), as recommended by the manufacturer. Second-round amplification was performed with REDTaq (Sigma-Aldrich, Dorset, United Kingdom) and 0.5 μmol/L forward (5′-GCA AGA ACT CAC AGG CCA GG-3′) and reverse (5′-GGG-CCA-CCC-TTC-GGA-GC-3′) primers using the following cycling parameters: 95°C for 5 minutes, 1 cycle; 95°C for 30 seconds; 65°C for 30 seconds; 72°C for 1 minute, 30 cycles; 72°C for 5 minutes. Each complementary DNA product was directionally cloned into TOPO II plasmid (Life Technologies, Carlsbad, CA), which incorporates T7 and SP6 RNA polymerase promoters flanking the cloning region defined by the *Xho*I or *Hin*dIII restriction enzyme site. Plasmids were sequenced, linearized, and transcribed with T7 (sense) or SP6 (antisense) RNA polymerases (Sigma) to yield digoxigenin-dUTP–labeled riboprobes in accordance with the manufacturer's protocol (Ambion, Life Technologies). Transcription was performed for 24 hours at 37°C. The template complementary DNA was digested away by RNase-free DNase (2 μL, 15 minutes), and the riboprobes were purified (Megaclear Purification and Filtration System; Ambion) and quantified by spectrophotometry and electrophoresis.

TABLE 2. Astroglia Ratios in All Regions

Region	Control	WMI	p Value
MD	0.16 ± 0.031	0.44 ± 0.039	*
VLp	0.15 ± 0.045	0.43 ± 0.050	*
VPL	0.23 ± 0.045	0.37 ± 0.050	ns
PLIC-VLp	0.31 ± 0.032	0.64 ± 0.070	*
PLIC-VPL	0.28 ± 0.061	0.53 ± 0.043	†

Data are expressed as mean ± SE.
Ratios are expressed as GFAP-positive cells/total cells.
* $p < 0.01$, difference in means between WMI and control.
† $p < 0.05$, difference in means between WMI and control.
ns, not significant.

In Situ Hybridization Procedure

Riboprobes (0.1 mg/mL) were denatured (5 minutes, 90°C) and added to hybridization buffer (50% formamide, Denhardt solution 50 g, 5× saline-sodium citrate, and salmon sperm DNA 40 μg/mL; Sigma-Aldrich Co Ltd, St Louis, MO). Tissue sections were processed as described previously (30). Sections were permeabilized with proteinase K (1–10 μg/mL, 37°C, 5 minutes; Sigma-Aldrich Co Ltd), postfixed in 4% paraformaldehyde, and blocked in hybridization buffer (10 minutes, 80°C) to prevent nonspecific binding. Sections were incubated with denatured riboprobes (200 μL per section), and hybridization was allowed to continue overnight (58°C). After hybridization, the sections were equilibrated in 5× saline-sodium citrate (15 minutes, room temperature; NaCl 0.75 mol/L and Na-citrate 0.075 mol/L) and washed in 2× saline-sodium citrate (30 minutes, 65°C). Afterward, the sections were placed in alkaline phosphatase buffer-1 (Tris-HCl 0.1 mol/L [pH 9.2], NaCl 0.1 mol/L, and $MgCl_2$ 0.5 mmol/L) for 10 minutes and incubated for 2 hours at room temperature with an alkaline phosphatase buffer-1–coupled anti-digoxigenin antibody cocktail (1:500; Roche Diagnostics Corp, Indianapolis, IN) containing a 0.5% bovine serum albumin blocking reagent. Sections were rinsed for 10 minutes in alkaline phosphatase buffer-1 followed by 2 × 5-minute rinses in alkaline phosphatase buffer-2 (Tris-HCl 0.1 mol/L [pH 9.2], NaCl 0.1 mol/L, and $MgCl_2$ 50 mmol/L) and visualized in nitro blue tetrazolium in dimethylformamide and 5-bromo-4-chloro-3-indolyl phosphate solution (Roche Diagnostics Corp) in 10 mL of alkaline phosphatase buffer-2 with levamisole 1 mmol/L (Sigma-Aldrich Co Ltd). The sense probe was used as negative control for specificity.

RESULTS

Glial Cell Morphology and Neuronal Counts Differ Between WMI Cases and Controls

We first evaluated total cell count with each assessment of glia populations and neurons in control cases and in cases with WMI. There was no difference in the average cell density in thalamic regions or white matter regions between control cases and WMI cases (Fig. 1B). We established that gestational age or postmenstrual age had no effect on the total number of cells in our regions of interest within the thalamus or white matter regions, regardless of the presence of WMI (Supplemental Digital Content 1, http://links.lww.com/NEN/A703; Data, Supplemental Digital Content 2, http://links.lww.com/NEN/A704). However, there was a significant increase in the ratio of astrocytes to total cell count in thalamic regions in WMI cases, compared with MD ($p < 0.01$) and VLp ($p < 0.01$)—but not VPL—thalamic regions in control cases. The astroglia ratio increased in the corresponding white matter regions, PLIC-VLp ($p < 0.01$) and PLIC-VPL ($p < 0.05$), in WMI cases compared with controls (Table 2). Astroglia were hypertrophic with fibrous and long extensive processes (Fig. 2B) in WMI cases compared with those seen in the control group (Fig. 2A).

Next, we assessed Iba-1–positive microglial cells and identified a significant increase in WMI cases in the MD ($p < 0.01$), VLp ($p < 0.01$), and VPL ($p < 0.05$) thalamic regions

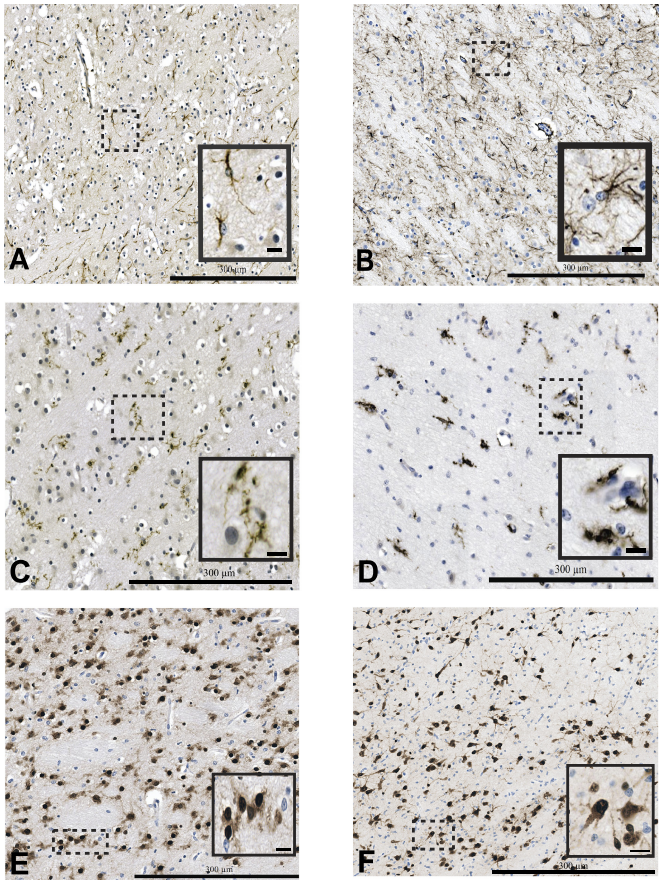

FIGURE 2. Glial and neuronal staining in VLp thalamic nuclei. Astrocytes are less fibrous and less reactive in controls **(A)** than in WMI cases **(B)**. The astroglia ratio in the total cell population in the MD region ($p < 0.01$), VLp region ($p < 0.01$), and adjacent PLIC regions (PLIC-VLp nuclei, $p < 0.01$; PLIC-VPL nuclei, $p < 0.05$) was significantly different between WMI cases and control cases. Different morphologies of microglia are seen in the VLp thalamic region between controls (intermediate; **C**) and WMI cases (amoeboidal; **D**). The microglia ratio increases significantly in the MD ($p < 0.01$), VLp ($p < 0.01$), and VPL ($p < 0.05$) regions and in PLIC-VPL. A decreased number of neurons in the MD ($p < 0.05$), VLp ($p < 0.005$), and VPL ($p < 0.05$) regions were seen in WMI cases **(F)** compared with controls **(E)**. Scale bars = **(A–F)** 300 μm; (insets) 10 μm.

and in the adjacent white matter region PLIC-VPL ($p < 0.05$), but not in PLIC-VLp (Table 3). Microglia in control cases were more consistent with an intermediate morphology (with extensive complex branching and ruffling; Fig. 2C), whereas in WMI cases, microglia consisted of amoeboidal (round to amorphous structures with a variety of short pseudopodia) and intermediate morphologies (Fig. 2D).

Finally, we counted the HuC/HuD-positive neuronal population in the thalamic and PLIC regions. There was a significant decrease in neurons in WMI cases in the MD ($p < 0.05$), VLp ($p < 0.005$), and VPL ($p < 0.05$) thalamic regions. However, we found that, in the WMI group, there was a significant increase in neurons detected in PLIC-VPL ($p < 0.05$), but not in PLIC-VLp (Table 4). Controls had mossy fibrous extensions protruding from cell bodies (Fig. 2E). In WMI cases, there were less fine fibrous protrusions extending from neuronal cell bodies, but axonal extensions were well defined (Fig. 2F).

Messenger RNA Expression of TLR3 Is Widespread in WMI

Using in situ hybridization, we compared TLR3 messenger RNA (mRNA) expression in the VLp thalamic region between control cases and WMI cases. In controls, the VLp region of the thalamus had faint cytoplasmic TLR3 mRNA expression (Fig. 3A), whereas in WMI cases, the cytoplasmic mRNA expression of TLR3 was very dense and granular, which may be indicative of upregulation of TLR3 expression in response to the surrounding injury (Fig. 3B).

Areas of TLR3 Immunoreactivity Are Increased in WMI

The density of TLR3 mRNA differed between WMI cases and controls. To ascertain whether this translated to a change in TLR3 protein expression, we measured the area of immunoreactivity. There was a significant increase in TLR3 positivity in WMI cases compared with controls in the MD ($p < 0.05$), VLp ($p < 0.05$), and VPL ($p < 0.01$) thalamic regions and in the adjacent white matter regions PLIC-VLp ($p < 0.05$) and PLIC-VLp ($p < 0.05$) (Table 5). Among neurons in thalamic regions (MD, VLp, and VPL) and neurons in PLIC, TLR3 immunoreactivity was globular and had a ribbon-like formation in the perinuclear region in control cases (Fig. 3C). Although WMI cases also showed TLR3 expression, there was more punctate and granular staining seen outside the nucleus of cells and extending along processes, in contrast to the more sporadic localization seen in noninjured brains (Fig. 3D). TLR3 was identified in the glutamatergic axonal region of Round Large glutamatergic neurons (34) in controls (Fig. 3E) and WMI cases (Fig. 3F). In contrast, TLR3 was not identified within GABAergic neurons in the VLp thalamic region in controls (Fig. 3G) and WMI cases (Fig. 3H).

TABLE 3. Microglia Ratio in All Regions

Region	Control	WMI	p Value
MD	0.076 ± 0.01	0.25 ± 0.050	*
VLp	0.038 ± 0.009	0.22 ± 0.040	*
VPL	0.044 ± 0.006	0.19 ± 0.059	†
PLIC-VLp	0.120 ± 0.022	0.17 ± 0.009	ns
PLIC-VPL	0.076 ± 0.021	0.25 ± 0.050	†

Data are expressed as mean ± SE.
Ratios are expressed as Iba-1–positive cells/total cells.
* $p < 0.01$, difference in means between WMI and control.
† $p < 0.05$, difference in means between WMI and control.
ns, not significant.

TABLE 4. Neuron Ratios in All Regions

Region	Control	WMI	p Value
MD	0.55 ± 0.053	0.36 ± 0.026	*
VLp	0.61 ± 0.053	0.33 ± 0.021	†
VPL	0.55 ± 0.048	0.37 ± 0.020	*
PLIC-VLp	0.12 ± 0.013	0.16 ± 0.013	ns
PLIC-VPL	0.10 ± 0.015	0.19 ± 0.028	‡

Data are expressed as mean ± SE.
Ratios are expressed as HuC/HuD-positive cells/total cells.
* $p < 0.05$, difference in means between WMI versus control.
† $p < 0.005$, difference in means between WMI versus control.
‡ $p < 0.01$, difference in means between WMI versus control.
ns, not significant.

IRF-3 Expression Is Perinuclear in Controls But Nuclear in WMI Cases

Because the most substantial differences between WMI cases and control cases were observed in the VLp region (i.e. higher ratio of astrocytes and microglia with lower ratio of neurons), we focused on this region to further investigate TLR3 signaling. Translocation of IRF-3 from the cytosol to the nucleus is a reported consequence of TLR3 signaling (20). Because there was upregulation in the expression of TLR3 postinjury (Fig. 3), we used IRF-3 translocation as a surrogate to investigate whether the increased expression correlated with increased TLR3 function. To evaluate nuclear IRF-3 expression in the VLp thalamus, we defined the nuclear boundary with DAPI staining and measured the amount of immunoreactivity of anti–IRF-3 antibodies. We found that nuclear IRF-3 expression was markedly increased in WMI cases compared with controls (WMI, 51.4 ± 9.97, n = 7; controls, 7.2 ± 1.4, n = 7; $p < 0.01$; Figs. 4A–C). This suggests that TLR3 elicited more IRF-3 activation in WMI cases compared with controls.

TLR3 Is More Prevalent in the ER in WMI

Toll-like receptor-3 is known to be synthesized in the ER (20). To study whether WMI altered the production of TLR3, we performed immunofluorescence colocalization studies using TLR3 and an ER marker, calreticulin, in the VLp thalamic region. Toll-like receptor-3 expression was frequently identified with ER surfaces in WMI cases. Toll-like receptor-3 in control cases was sparsely identified in the ER but could be seen weaving alongside the convolutions but not attached to the ER. There was a significant increase in the colocalization of the ER (Fig. 5C) and TLR3 ($p < 0.01$) identified in the WMI group (Fig. 5B) compared with the control group (Fig. 5A).

TLR3 Is Found in Late Endosomes in Controls and WMI Cases

Because TLR3 is known to translocate to endosomes on stimulation and because we observed an increase in the

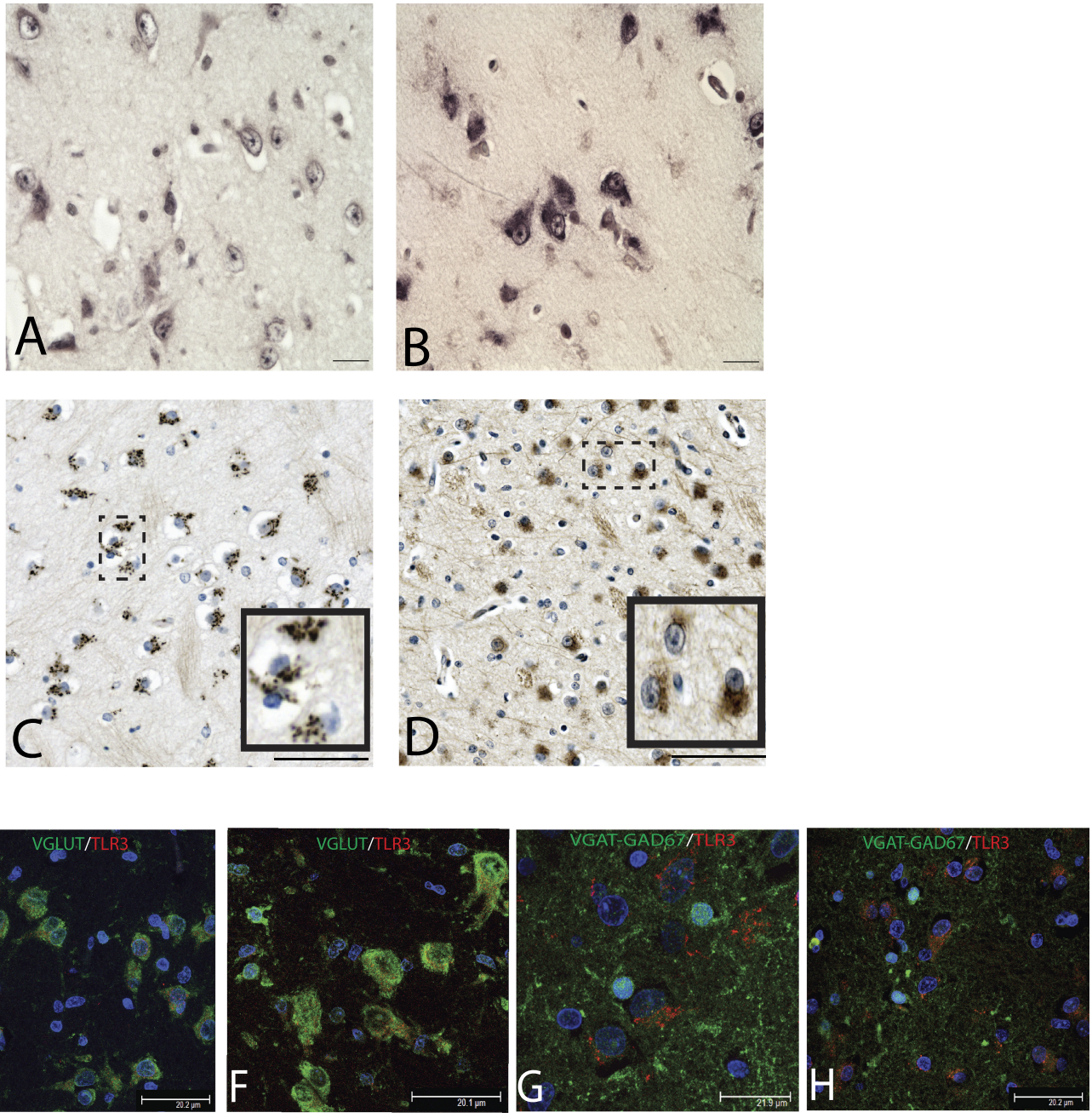

FIGURE 3. (A, B) In situ hybridization of TLR3 in the VLp thalamus. TLR3 mRNA was detected mainly in neurons. **(A)** TLR3 mRNA expression was very punctate in controls, whereas TLR3 in situ hybridization was dark and granular in WMI cases **(B)**. **(C, D)** Protein expression of TLR3 in VLp thalamic nuclei in cases with and without WMI. In a case without any known pathology, staining was globular and perinuclear **(C)**, whereas in a case with WMI, staining had a granular and diffuse morphology **(D)**. White matter injury cases had a significant increase in the area (μm^2) of TLR3 immunoreactivity in all regions of interest (MD nuclei, $p < 0.05$; VLp nuclei, $p < 0.05$; VPL nuclei, $p < 0.01$; white matter in PLIC-VLp, $p < 0.05$; white matter in VPL, $p < 0.05$). Double labeling for TLR3 and glutamate synaptic vesicle protein (vesicular glutamate transporter-1 [VGLUT-1]) shows that TLR3 is more widely expressed in glutamatergic neuronal processes (VGLUT-1; **E**, control; **F**, WMI case) than in GABergic neurons processes identified with anti–glutamate decarboxylase-67 (GAD67) and anti–vesicular GABA transporter (VGAT; **G**, control; **H**, WMI). Scale bars = **(A, B, E–H)** 20 μm; **(D, C)** 100 μm.

TABLE 5. TLR3-Immunopositive Areas

Region	Control	WMI	p Value
MD	22 ± 2.3	62 ± 12	*
VLp	26 ± 5.4	63 ± 6.8	*
VPL	23 ± 4.4	65 ± 12	†
PLIC-VLp	8.9 ± 2.5	45 ± 4.5	*
PLIC-VPL	18 ± 3.1	54 ± 8.3	*

Data are expressed as mean ± SE.

Ratios are expressed as TLR3 immunoreactivity areas (μm^2) in WMI cases and controls.

* $p < 0.05$.

† $p < 0.01$.

expression of TLR3 in the ER in WMI (Fig. 5B), we performed colocalization studies of TLR3 with early endosomal antigen-1 and late endosome markers (lysosome-associated membrane protein-1 [LAMP-1]). In contrast with previous studies using dendritic cells (20), we found that TLR3 expression colocalized with late endosomal makers ($p < 0.05$; LAMP-1), but not with early endosomal antigen-1 (data not shown). Colocalization between LAMP-1 and TLR3 was significantly higher in WMI cases (Fig. 5E) compared with controls (Fig. 5D), suggesting that WMI stimulates excessive DAMP production and, as a consequence, upregulates the necessary clearance mechanisms (Fig. 5F).

Increase in Autophagy in WMI

Besides showing the role of TLR3 in endosome-mediated degradation, very recent studies have implicated Toll/IL-1–inducing interferon-β nuclear and, by association, TLR3 in autophagy (35–37). Indeed, another nucleic acid–sensing TLR, TLR9, has been implicated in a noncanonical autophagy pathway known as microtubule-associated protein light chain–associated phagocytosis, where rapid recruitment of microtubule-associated protein light chain to phagosomes facilitates fusion with lysosomes (35, 38). Therefore, we examined the colocalization of TLR3 with microtubule-associated protein light chain 3B (LC-3-II), a marker of autophagosome formation. In all of the cases, TLR3 colocalized with the LC-3-II marker of autophagy, but there was no difference in the degree of colocalization (Fig. 6G) between WMI cases (Fig. 6D) and controls (Fig. 6A).

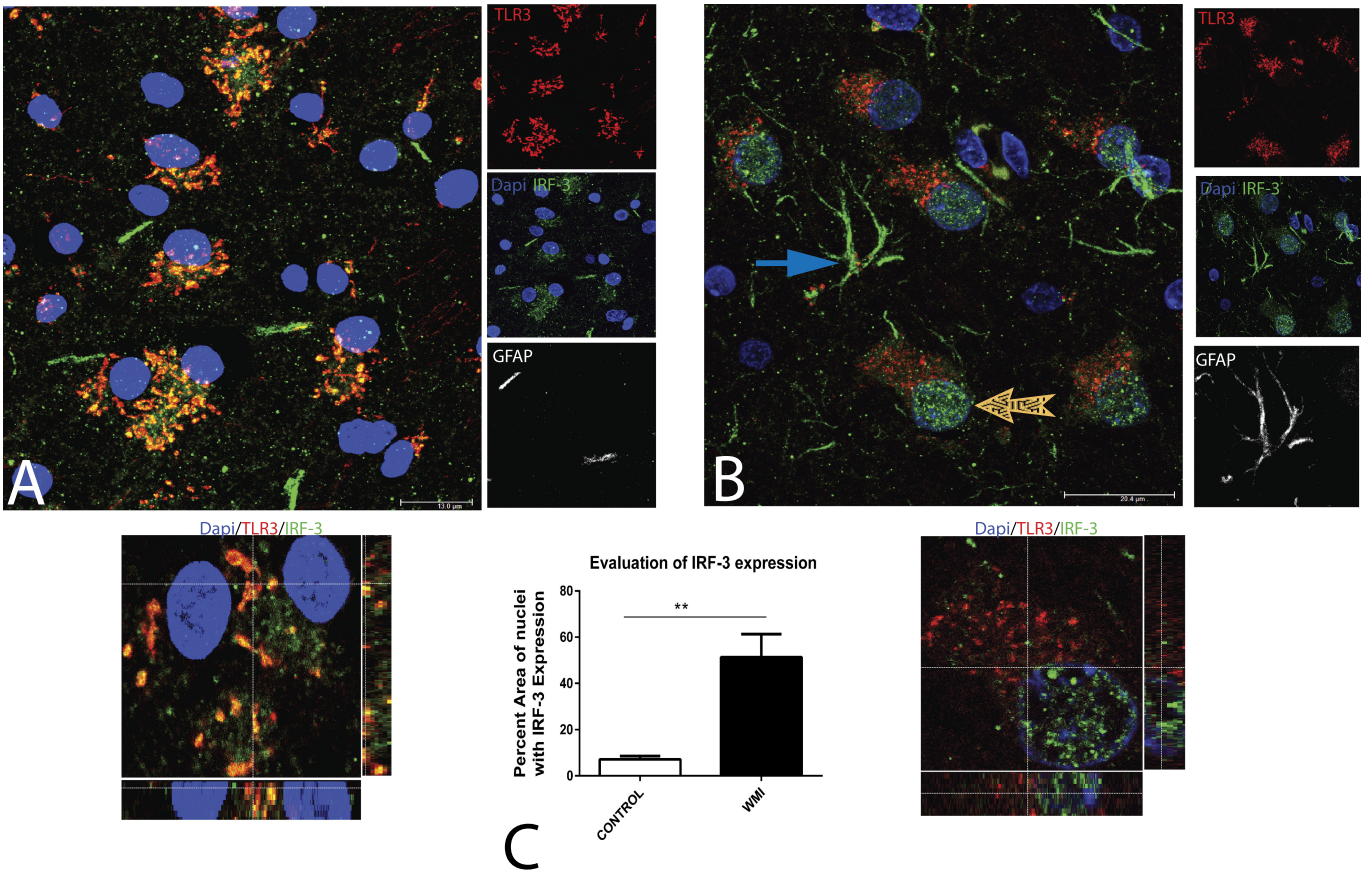

FIGURE 4. Localization of IRF-3. Immunoreactivity of IRF-3 (green) and TLR3 (red) in a control **(A)** and a WMI case **(B)**. **(A)** Expression of IRF-3 is outside the nuclei (DAPI; blue), whereas IRF-3 expression is more nuclear (yellow arrowhead) in the WMI case **(B)**. The blue arrow points to IRF-3–positive structures that colocalize with astrocyte processes in the WMI case. Side panels show separate channels for TLR3, IRF-3 with DAPI, and GFAP. The panels below the images are orthogonal views imaged within the *z*-plane. **(C)** Graph illustrates an increase in the percent area of nuclei that has IRF-3 expression in WMI cases compared with control cases. ** $p < 0.01$. Scale bars = **(A)** 13 μm; **(B)** 20 μm.

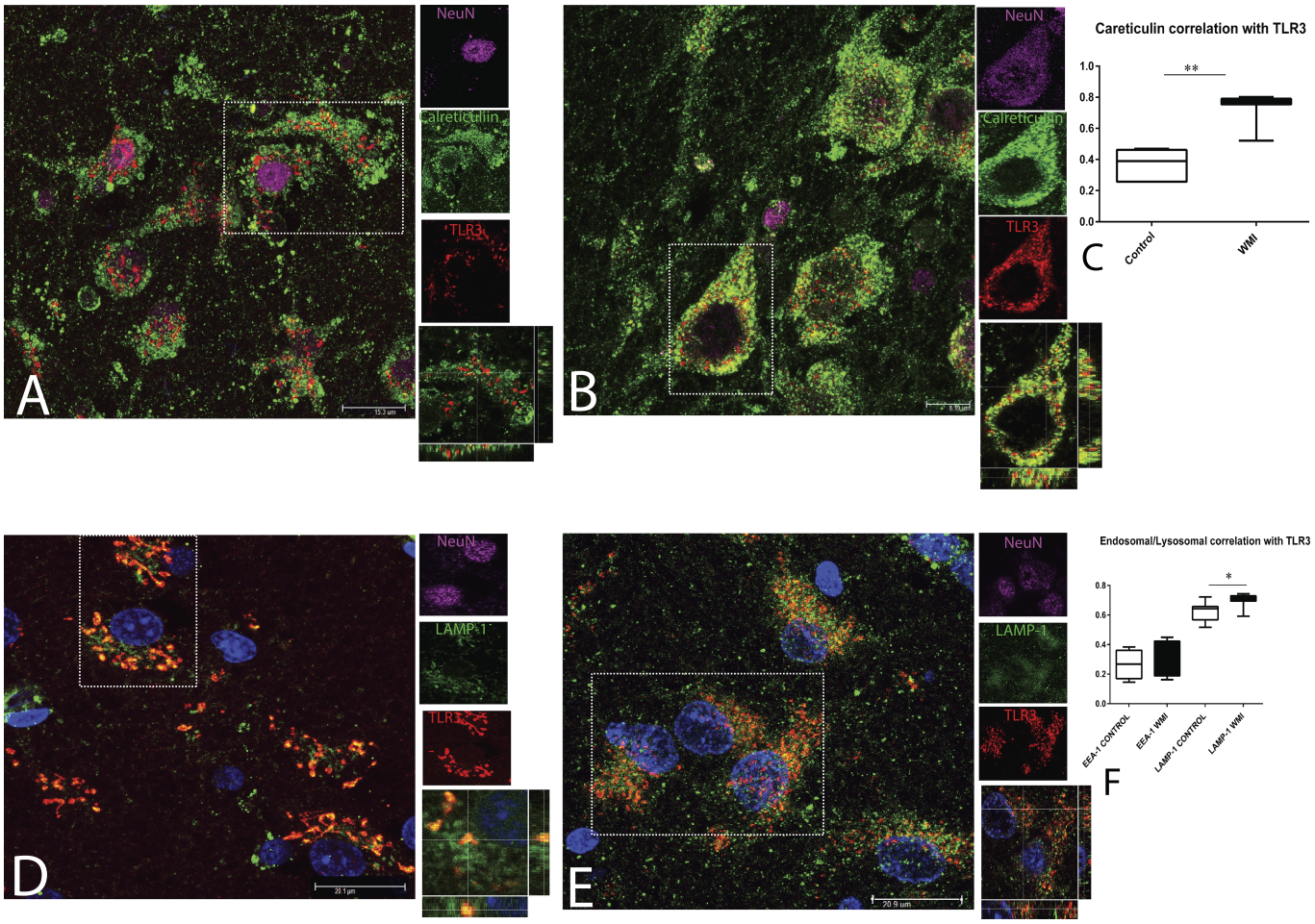

FIGURE 5. Confocal photomicrographs demonstrating the colocalization of TLR3 within the ER and late endosomes. Confocal images with anti-TLR3 (red) and an ER marker (green; anti-calreticulin) differ between controls **(A)** and WMI **(B)** cases. The average correlation value for the TLR3-calreticulin overlap in WMI cases is significantly higher than that observed in controls **(C)** (** $p < 0.01$). In contrast, TLR3 and the late endosomal marker (LAMP-1; green) from the ventrolateral region of the thalamus colocalize in control cases **(D)** and WMI cases **(E)**. Toll-like receptor-3 is more prevalent in late endosomes than in early endosomes (**F**; * $p < 0.05$). Anti-NeuN (neuronal marker; purple) was added to identify neurons and is shown in the side panels along with individual antigens and the orthogonal view. Scale bars = **(A)** 15 μm; **(B)** 8 μm; **(D, E)** 20 μm. EEA-1, early endosome antigen-1.

An increase in the staining of LC-3-II was observed in WMI cases compared with controls, suggesting not only that TLR3 is localized on the autophagosome but also that WMI may increase autophagy as a possible alternative protective mechanism.

Mitophagy Increases After WMI

Finally, because autophagy seemed to be upregulated in WMI, we determined whether a subset of this recycling mechanism (mitophagy) was also altered. Mitochondrial dysfunction has been implicated in the development of brain injury in term and preterm infants (39), and mitochondria have had an increasing role as a platform for innate immunity (12, 40). Mitophagy (or recycling of damaged mitochondria) would therefore represent a potential mechanism for cell survival. Therefore, we assessed the colocalization of LC-3-II, TLR3, and mitochondrial antigen. Interestingly, we found that there was a significant increase in the colocalization of anti–LC-3-II immunoreactivity with TLR3 and mitochondria in WMI ($p < 0.001$; Figs. 6H, I), suggesting that, after WMI has occurred, induced autophagy (a catabolic response) occurs to free the cell of damaged proteins and organelles, including mitochondria.

DISCUSSION

In this study, we have identified TLR3 expression in different cellular components of neurons in the preterm neonatal human brain; to the best of our knowledge, this is the first time that this family of receptors has been demonstrated in neurons of the thalamus in the neonatal human brain. Our results are compatible with the model outlined in Figure 7, which describes how TLR3 responds to an increase in endogenous DAMPs being released after WMI has occurred. It is still unknown whether there is a cause-effect relationship between WMI and TLR3 alterations in the thalamus, or whether the exposure causing WMI also induces cellular stress in thalamic nuclei with subsequent changes in TLR3. We showed that, in the neurons of the VLp thalamus, there was an increase in

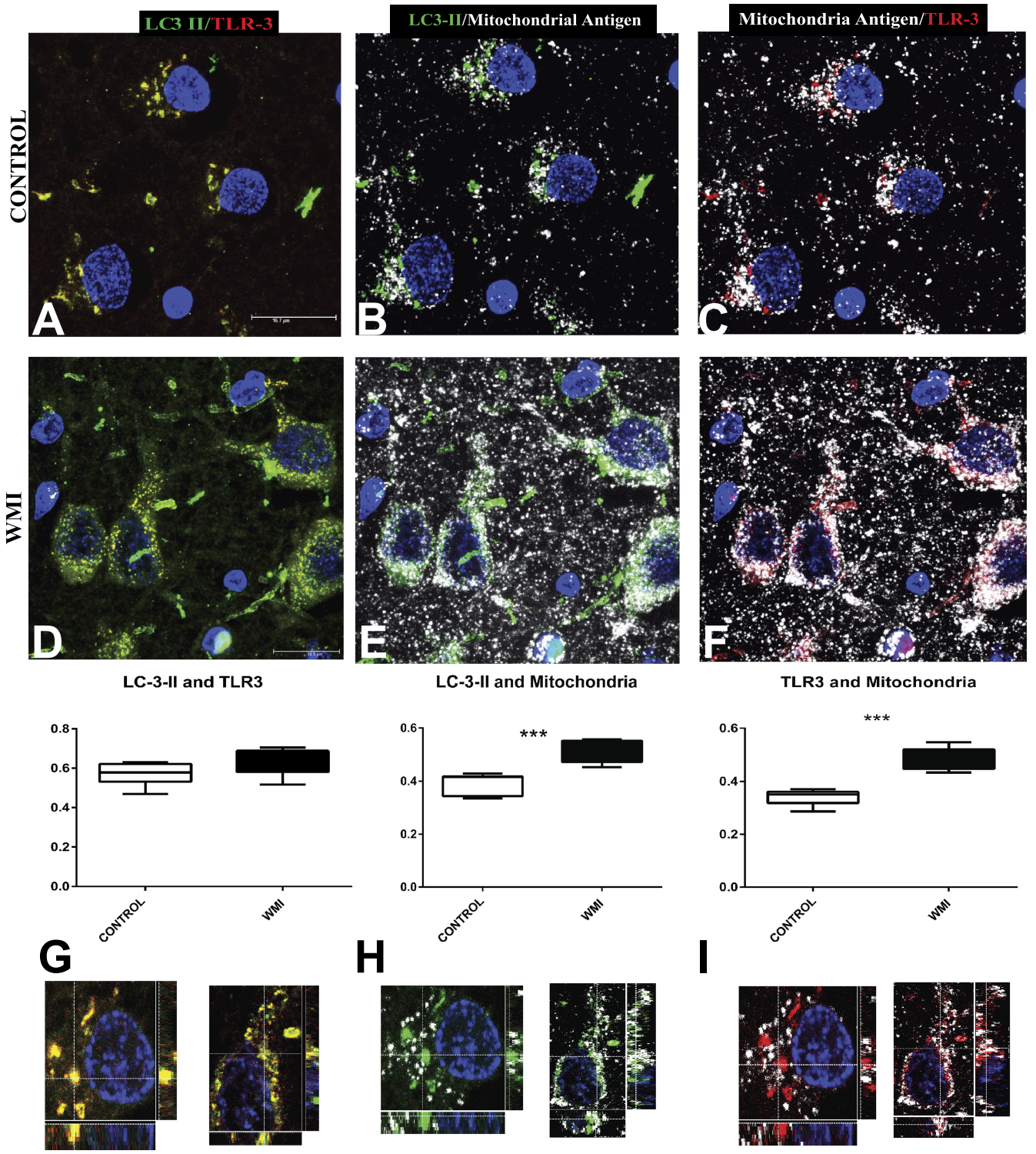

FIGURE 6. Confocal photomicrographs demonstrating the distribution of TLR3 (red), anti–microtubule-associated protein light chain (LC-3-II) (green), and mitochondria (anti–mitochondrial antigen; white) from the VLp thalamic region in a control case **(A–C)** and a WMI case **(D–F)**. The immunoreactivity of LC-3-II increased after WMI, but LC-3-II and TLR3 equally colocalized **(G)** in WMI cases **(D)** and controls **(A)**. The colocalization of LC-3-II and mitochondria is significantly higher in WMI cases **(E)** than in controls **(B)**, suggesting that mitophagy may be occurring **(H)**. In the control case, TLR3 is located densely around the nucleus but does not colocalize with the mitochondria **(C)**, whereas in the WMI case, TLR3 expression seems to be localized with the mitochondria but only in conjunction with LC-3-II expression **(F, I)**. *** $p < 0.001$. Bottom images show orthogonal views within the z-stack. Scale bars = **(A–C)** 16 μm; **(D–F)** 14 μm.

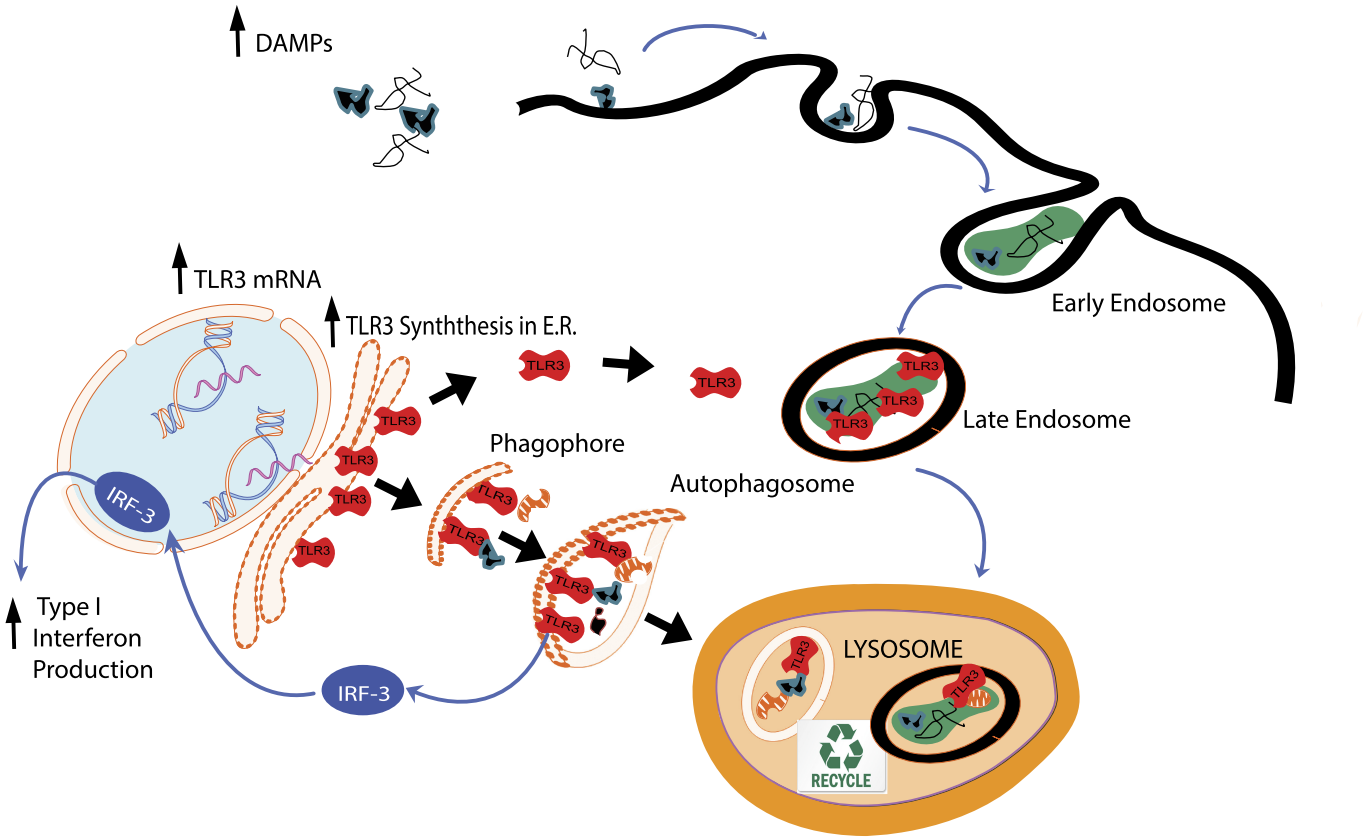

FIGURE 7. Cartoon depicting the proposed pathway of TLR3 activation after WMI and in controls. TLR3 are synthesized in the ER. TLR3 production is increased in response to DAMPs and stays on ER fragments that are recruited to form phagophores. The phagophore elongates, forming the microtubule-associated protein light chain (LC-3-II)–positive autophagosome, which engulfs DAMPs and fuses with the lysosome, where components such as mitochondria are recycled. TLR3 is upregulated in the ER and autophagosomal components in response to WMI, suggesting that another method of cellular adaptation to WMI may include autophagy. Another pathway for recycling damaged components is via endosomes. As endosomes mature, TLR3 is recruited to late endosomes (LAMP-1), and components of macromolecules are acidified as they fuse with the lysosome. TLR3 is present in endosomes in control and WMI tissues, where it responds to DAMPs. This response is exaggerated after WMI. Activation of TLR3 also results in the recruitment, nuclear translocation, and subsequent activation of IRF-3, which regulates the production of type I interferons.

the mRNA expression of TLR3, which translated to protein synthesis in the ER in cases with WMI. Furthermore, there was an increase in autophagy and lysosomal proteins in WMI cases, whereas in controls, TLR3 mainly colocalized with late endosomes. Moreover, these findings imply that neuronal TLR3 increased and was activated via the Toll/IL-1–inducing interferon-β nuclear pathway because IRF-3 was translocated to the nucleus in association with adjacent WMI.

Gestational ages at birth were similar in the WMI and control groups, but survival was longer in the WMI group. We cannot exclude the possibility that WMI would have developed in some control cases had they lived longer, but we looked at a very early time point before any established disease could be detected. Nevertheless, our data suggest that TLR3 expression was altered in the presence of overt WMI in the preterm brain.

Thalamic Nuclei Segregation and Pathologic Findings

Previous studies focused on the MD region have shown that atrophy in the thalamus is associated with selective microstructural abnormalities (41). Although segregating the different regions of the ventral thalamic nuclei is an arduous undertaking (32, 42), we were able to use lateral anatomic landmarks from the globus pallidum and the established cytoarchitecture (31) of the different thalamic regions to define 3 regions of interest. It is imperative that future histologic investigations on preterm neurologic function include defined thalamic regions. For example, reductions of the MD and pulvinar thalamic regions have been strongly associated with abnormal cognitive outcomes and have been identified in preterm infants with WMI (8, 10). Preterm birth also is associated with a high risk of a range of motor impairments, and the severity of motor impairments increases with WMI (43) in part because the sites of periventricular infarcts lie in the motor pathways (44). Hence, after WMI has occurred in preterm neonates, there may be pathologic processes in specific thalamic regions that may be correlated with cognitive and motor impairments.

Our investigation substantiates the findings of other studies that have identified abnormalities in the thalamus of

preterm infants with WMI. Ligam et al (10) found reactive astrocytes in the MD region and in the reticular nucleus (a structure that surrounds and modulates the lateral thalamic nuclei [32] with GABAergic neurons) of preterm postmortem cases with WMI. In the present study, we demonstrate an increase in the ratio of astrocytes in the MD and VLp thalamic nuclei to astrocytes in adjacent PLIC among WMI cases.

Normally in gray matter, protoplasmic astrocytes exhibit short and highly branched processes and possess a large quantity of organelles. In WMI cases, astroglia were hypertrophic, with extensive processes and greater expression of GFAP, which is indicative of a reactive form that may promote a prolonged proinflammatory response (45, 46).

In conjunction with an increase in astroglia, we found an increase in microglia in MD, VLp, and VPL thalamic nuclei and in PLIC-VPL in WMI cases. These findings are in line with previous studies that correlated pathology in the surrounding white matter structures with abnormalities seen in the thalamus (8, 47). In inflammatory injury of the preterm brain, such as in WMI, there is an influx of activated microglia (48). Microglia and astroglia respond to the injury and, on activation, release proinflammatory cytokines such as tumor necrosis factor, interleukin-6, interferon-γ, and nitric oxides (49).

As glial cells increased, we observed decreases in the neuronal populations in MD, VLp, and VPL thalamic nuclei in WMI cases. The neuronal loss in VLp nuclei substantiates studies of preterm cases that described WMI as impairing motor coordination of the limbs (43). Residual damage fragments released during WMI (or some cell injury locally in the thalamus) may continuously activate TLR3 as it responds to endogenous stimuli (50) in neuronal and astroglial populations (51). Further studies correlating thalamic abnormalities warrant more detailed investigation to comprehend motor and cognitive deficits associated with preterm pathologies.

TLR3 Molecular Mechanism

Previously, Johnsen et al (20) found that c-Src tyrosine kinase in dendritic cells is activated by dsRNA viral stimuli in the ER, where it recruits TLR3, mediates TLR3 translocation to endosomes, and induces various signaling cascades. The ER contains resident proteins such as calnexin and calreticulin (52), which serve as chaperones; unstimulated TLR3 was shown to colocalize with these resident proteins. Stimulated TLR3 colocalized with LAMP-1, which identifies late endosomes and lysosomes (20). Another possible platform for TLR3 activation is the phagaphore, which works in conjugation with LC-3-II to form the autophagosome (an important mediator to autophagy and mitophagy, i.e. degradation of damaged proteins and dysfunctional mitochondria) (12, 22, 53).

We have demonstrated that TLR3 was present in endosomes in controls and WMI cases and colocalized with LAMP-1, most likely as part of molecular surveillance for extracellular DAMPs and pathogen-associated molecular patterns. Another source of surveillance and degradation may be autophagy, as TLR3 colocalized with LC-3-II. Expression of LC-3-II increased in WMI; autophagy is particularly important in long-lived cells like neurons, and impairments in autophagy are associated with abnormal central nervous system development and neurologic impairment (12).

In conclusion, identifying changes in TLR3 expression associated with WMI may improve our understanding of the molecular mechanisms associated with impaired development in preterm infants.

ACKNOWLEDGMENTS

We thank the UK Medical Research Council for the use of human tissue samples. We would also like to thank Chloe Suzanne Atkins and Megan Holly Atkins, student volunteers from the Everest Community Academy (Basingstoke, United Kingdom) and Peter Symonds College (Winchester, United Kingdom), respectively, for their diligent work with cell counting and colocalization testing.

REFERENCES

1. Inder T, Neil J, Yoder B, et al. Patterns of cerebral injury in a primate model of preterm birth and neonatal intensive care. J Child Neurol 2005; 20:965–67
2. Ajayi-Obe M, Saeed N, Cowan FM, et al. Reduced development of cerebral cortex in extremely preterm infants. Lancet 2000;356:1162–63
3. Northington FJ, Traystman RJ, Koehler RC, et al. GLT1, glial glutamate transporter, is transiently expressed in neurons and develops astrocyte specificity only after midgestation in the ovine fetal brain. J Neurobiol 1999;39:515–26
4. Back S, Volpe J. Cellular and molecular pathogenesis of periventricular white matter injury. Ment Retard Dev Disabil Res Rev1997;3:96–107
5. Nagasunder AC, Kinney HC, Bluml S, et al. Abnormal microstructure of the atrophic thalamus in preterm survivors with periventricular leukomalacia. AJNR Am J Neuroradiol 2011;32:185–91
6. Graham EM, Sheldon RA, Flock DL, et al. Neonatal mice lacking functional Fas death receptors are resistant to hypoxic-ischemic brain injury. Neurobiol Dis 2004;17:89–98
7. Martinez-Biarge M, Diez-Sebastian J, Rutherford MA, et al. Outcomes after central grey matter injury in term perinatal hypoxic-ischaemic encephalopathy. Early Hum Dev 2010;86:675–82
8. Zubiaurre-Elorza L, Soria-Pastor S, Junque C, et al. Gray matter volume decrements in preterm children with periventricular leukomalacia. Pediatr Res 2011;69:554–60
9. de Vries LS, van Haastert IC, Benders MJ, et al. Myth: Cerebral palsy cannot be predicted by neonatal brain imaging. Semin Fetal Neonatal Med 2011;16:279–87
10. Ligam P, Haynes RL, Folkerth RD, et al. Thalamic damage in periventricular leukomalacia: Novel pathologic observations relevant to cognitive deficits in survivors of prematurity. Pediatr Res 2009;65:524–29
11. Thornton C, Rousset CI, Kichev A, et al. Molecular mechanisms of neonatal brain injury. Neurol Res Int 2012;2012:506320. doi: 10.1155/2012/506320 [Epub ahead of print]
12. Hagberg H, Mallard C, Rousset CI, et al. Mitochondria: Hub of injury responses in the developing brain. Lancet Neurol 2014;13:217–32
13. Johnston MV, Fatemi A, Wilson MA, et al. Treatment advances in neonatal neuroprotection and neurointensive care. Lancet Neurol 2011;10: 372–82
14. Botos I, Segal DM, Davies DR. The structural biology of Toll-like receptors. Structure 2011;19:447–59
15. Hagberg H, Gressens P, Mallard C. Inflammation during fetal and neonatal life: Implications for neurologic and neuropsychiatric disease in children and adults. Ann Neurol 2012;71:444–57
16. Harashima N, Inao T, Imamura R, et al. Roles of the PI3K/Akt pathway and autophagy in TLR3 signaling–induced apoptosis and growth arrest of human prostate cancer cells. Cancer Immunol Immunother 2012;61: 667–76
17. Lee BL, Barton GM. Trafficking of endosomal Toll-like receptors. Trends Cell Biol 2014;24:360–69

18. Kim YM, Brinkmann MM, Paquet ME, et al. UNC93B1 delivers nucleotide-sensing toll-like receptors to endolysosomes. Nature 2008; 452:234–38
19. Brinkmann MM, Spooner E, Hoebe K, et al. The interaction between the ER membrane protein UNC93B and TLR3, 7, and 9 is crucial for TLR signaling. J Cell Biol 2007;177:265–75
20. Johnsen IB, Nguyen TT, Ringdal M, et al. Toll-like receptor 3 associates with c-Src tyrosine kinase on endosomes to initiate antiviral signaling. EMBO J 2006;25:3335–46
21. Akira S, Takeda K. Toll-like receptor signalling. Nat Rev Immunol 2004; 4:499–511
22. Sun R, Zhang Y, Lv Q, et al. Toll-like receptor 3 (TLR3) induces apoptosis via death receptors and mitochondria by up-regulating the transactivating p63 isoform alpha (TAP63alpha). J Biol Chem 2011;286: 15918–28
23. He S, Liang Y, Shao F, et al. Toll-like receptors activate programmed necrosis in macrophages through a receptor-interacting kinase-3–mediated pathway. Proc Natl Acad Sci U S A 2011;108:20054–59
24. Kaiser WJ, Offermann MK. Apoptosis induced by the toll-like receptor adaptor TRIF is dependent on its receptor interacting protein homotypic interaction motif. J Immunol 2005;174:4942–52
25. Lathia JD, Okun E, Tang SC, et al. Toll-like receptor 3 is a negative regulator of embryonic neural progenitor cell proliferation. J Neurosci 2008;28:13978–84
26. Cameron JS, Alexopoulou L, Sloane JA, et al. Toll-like receptor 3 is a potent negative regulator of axonal growth in mammals. J Neurosci 2007; 27:13033–41
27. Stridh L, Mottahedin A, Johansson ME, et al. Toll-like receptor-3 activation increases the vulnerability of the neonatal brain to hypoxia-ischemia. J Neurosci 2013;33:12041–51
28. Meyer U. Prenatal poly(i:C) exposure and other developmental immune activation models in rodent systems. Biol Psychiatry 2014;75:307–15
29. Meyer U, Feldon J. To poly(I:C) or not to poly(I:C): Advancing preclinical schizophrenia research through the use of prenatal immune activation models. Neuropharmacology 2012;62:1308–21
30. Vontell R, Supramaniam V, Thornton C, et al. Toll-like receptor 3 expression in glia and neurons alters in response to white matter injury in preterm infants. Dev Neurosci 2013;35:130–39
31. Sherman SM. The function of metabotropic glutamate receptors in thalamus and cortex. Neuroscientist 2013;20:136–49
32. Jones EG. *The Thalamus*. 2nd ed. Cambridge, United Kingdom: Cambridge University Press, 2007
33. Misselwitz B, Strittmatter G, Periaswamy B, et al. Enhanced CellClassifier: A multi-class classification tool for microscopy images. BMC Bioinformatics 2010;11:30. doi: 10.1186/1471-2105-11-30
34. Sherman SM, Guillery RW. *Functional Connections of Cortical Areas: A New View From the Thalamus*. London, England: The MIT Press, 2013
35. Oh JE, Lee HK. Pattern recognition receptors and autophagy. Front Immunol 2014;5:300
36. Xu Y, Liu XD, Gong X, et al. Signaling pathway of autophagy associated with innate immunity. Autophagy 2008;4:110–12
37. Zhan Z, Xie X, Cao H, et al. Autophagy facilitates TLR4- and TLR3-triggered migration and invasion of lung cancer cells through the promotion of TRAF6 ubiquitination. Autophagy 2014;10:257–68
38. Henault J, Martinez J, Riggs JM, et al. Noncanonical autophagy is required for type I interferon secretion in response to DNA-immune complexes. Immunity 2012;37:986–97
39. Rousset CI, Baburamani AA, Thornton C, et al. Mitochondria and perinatal brain injury. J Matern Fetal Neonatal Med 2012;25(Suppl 1):35–38
40. Liu QA, Shio H. Mitochondrial morphogenesis, dendrite development, and synapse formation in cerebellum require both Bcl-w and the glutamate receptor delta2. PLoS Genet 2008;4:e1000097
41. Zubiaurre-Elorza L, Soria-Pastor S, Junque C, et al. Thalamic changes in a preterm sample with periventricular leukomalacia: Correlation with white-matter integrity and cognitive outcome at school age. Pediatr Res 2012;71:354–60
42. Sherman SM, Guillery RW, Sherman SM. *Exploring the Thalamus and Its Role in Cortical Function*. 2nd ed. Cambridge, MA: MIT Press, 2006
43. Spittle AJ, Orton J. Cerebral palsy and developmental coordination disorder in children born preterm. Semin Fetal Neonatal Med 2014;19:84–89
44. Lagercrantz H. *The Newborn Brain: Neuroscience and Clinical Applications*. 2nd ed. Cambridge, United Kingdom: Cambridge University Press, 2010
45. Hagberg H, Mallard C. Effect of inflammation on central nervous system development and vulnerability. Curr Opin Neurol 2005;18:117–23
46. Kinney H, Back S. Human oligodendroglial development: Relationship to periventricular leukomalacia. Semin Pediatr Neonat 1997;5:180–89
47. Haynes RL, Xu G, Folkerth RD, et al. Potential neuronal repair in cerebral white matter injury in the human neonate. Pediatr Res 2011;69: 62–67
48. Supramaniam V, Vontell R, Srinivasan L, et al. Microglia activation in the extremely preterm human brain. Pediatr Res 2013;73:301–9
49. Rezaie P, Dean A. Periventricular leukomalacia, inflammation and white matter lesions within the developing nervous system. Neuropathology 2002;22:106–32
50. Kariko K, Ni H, Capodici J, et al. mRNA is an endogenous ligand for Toll-like receptor 3. J Biol Chem 2004;279:12542–50
51. Bsibsi M, Bajramovic JJ, Vogt MH, et al. The microtubule regulator stathmin is an endogenous protein agonist for TLR3. J Immunol 2010; 184:6929–37
52. Desjardins M. ER-mediated phagocytosis: A new membrane for new functions. Nat Rev Immunol 2003;3:280–91
53. Zhu C, Wang X, Xu F, et al. The influence of age on apoptotic and other mechanisms of cell death after cerebral hypoxia-ischemia. Cell Death Differ 2005;12:162–76

